Centrality Dependence of Direct Photon Production in $\sqrt{S_{NN}} = 200$ GeV Au + Au Collisions

S. S. Adler,[5] S. Afanasiev,[17] C. Aidala,[5] N. N. Ajitanand,[43] Y. Akiba,[20,38] J. Alexander,[43] R. Amirikas,[12] L. Aphecetche,[45] S. H. Aronson,[5] R. Averbeck,[44] T. C. Awes,[35] R. Azmoun,[44] V. Babintsev,[15] A. Baldisseri,[10] K. N. Barish,[6] P. D. Barnes,[27] B. Bassalleck,[33] S. Bathe,[30] S. Batsouli,[9] V. Baublis,[37] A. Bazilevsky,[39,15] S. Belikov,[16,15] Y. Berdnikov,[40] S. Bhagavatula,[16] J. G. Boissevain,[27] H. Borel,[10] S. Borenstein,[25] M. L. Brooks,[27] D. S. Brown,[34] N. Bruner,[33] D. Bucher,[30] H. Buesching,[30] V. Bumazhnov,[15] G. Bunce,[5,39] J. M. Burward-Hoy,[26,44] S. Butsyk,[44] X. Camard,[45] J.-S. Chai,[18] P. Chand,[4] W. C. Chang,[2] S. Chernichenko,[15] C. Y. Chi,[9] J. Chiba,[20] M. Chiu,[9] I. J. Choi,[52] J. Choi,[19] R. K. Choudhury,[4] T. Chujo,[5] V. Cianciolo,[35] Y. Cobigo,[10] B. A. Cole,[9] P. Constantin,[16] D. d'Enterria,[45] G. David,[5] H. Delagrange,[45] A. Denisov,[15] A. Deshpande,[39] E. J. Desmond,[5] A. Devismes,[44] O. Dietzsch,[41] O. Drapier,[25] A. Drees,[44] R. du Rietz,[29] A. Durum,[15] D. Dutta,[4] Y. V. Efremenko,[35] K. El Chenawi,[49] A. Enokizono,[14] H. En'yo,[38,39] S. Esumi,[48] L. Ewell,[5] D. E. Fields,[33,39] F. Fleuret,[25] S. L. Fokin,[23] B. D. Fox,[39] Z. Fraenkel,[51] J. E. Frantz,[9] A. Franz,[5] A. D. Frawley,[12] S.-Y. Fung,[6] S. Garpman,[29,*] T. K. Ghosh,[49] A. Glenn,[46] G. Gogiberidze,[46] M. Gonin,[25] J. Gosset,[10] Y. Goto,[39] R. Granier de Cassagnac,[25] N. Grau,[16] S. V. Greene,[49] M. Grosse Perdekamp,[39] W. Guryn,[5] H.-Å. Gustafsson,[29] T. Hachiya,[14] J. S. Haggerty,[5] H. Hamagaki,[8] A. G. Hansen,[27] E. P. Hartouni,[26] M. Harvey,[5] R. Hayano,[8] N. Hayashi,[38] X. He,[13] M. Heffner,[26] T. K. Hemmick,[44] J. M. Heuser,[44] M. Hibino,[50] J. C. Hill,[16] W. Holzmann,[43] K. Homma,[14] B. Hong,[22] A. Hoover,[34] T. Ichihara,[38,39] V. V. Ikonnikov,[23] K. Imai,[24,38] D. Isenhower,[1] M. Ishihara,[38] M. Issah,[43] A. Isupov,[17] B. V. Jacak,[44] W. Y. Jang,[22] Y. Jeong,[19] J. Jia,[44] O. Jinnouchi,[38] B. M. Johnson,[5] S. C. Johnson,[26] K. S. Joo,[31] D. Jouan,[36] S. Kametani,[8,50] N. Kamihara,[47,38] J. H. Kang,[52] S. S. Kapoor,[4] K. Katou,[50] S. Kelly,[9] B. Khachaturov,[51] A. Khanzadeev,[37] J. Kikuchi,[50] D. H. Kim,[31] D. J. Kim,[52] D. W. Kim,[19] E. Kim,[42] G.-B. Kim,[25] H. J. Kim,[52] E. Kistenev,[5] A. Kiyomichi,[48] K. Kiyoyama,[32] C. Klein-Boesing,[30] H. Kobayashi,[38,39] L. Kochenda,[37] V. Kochetkov,[15] D. Koehler,[33] T. Kohama,[14] M. Kopytine,[44] D. Kotchetkov,[6] A. Kozlov,[51] P. J. Kroon,[5] C. H. Kuberg,[1,27] K. Kurita,[39] Y. Kuroki,[48] M. J. Kweon,[22] Y. Kwon,[52] G. S. Kyle,[34] R. Lacey,[43] V. Ladygin,[17] J. G. Lajoie,[16] A. Lebedev,[16,23] S. Leckey,[44] D. M. Lee,[27] S. Lee,[19] M. J. Leitch,[27] X. H. Li,[6] H. Lim,[42] A. Litvinenko,[17] M. X. Liu,[27] Y. Liu,[36] C. F. Maguire,[49] Y. I. Makdisi,[5] A. Malakhov,[17] V. I. Manko,[23] Y. Mao,[7,38] G. Martinez,[45] M. D. Marx,[44] H. Masui,[48] F. Matathias,[44] T. Matsumoto,[8,50] P. L. McGaughey,[27] E. Melnikov,[15] F. Messer,[44] Y. Miake,[48] J. Milan,[43] T. E. Miller,[49] A. Milov,[44,51] S. Mioduszewski,[5] R. E. Mischke,[27] G. C. Mishra,[13] J. T. Mitchell,[5] A. K. Mohanty,[4] D. P. Morrison,[5] J. M. Moss,[27] F. Mühlbacher,[44] D. Mukhopadhyay,[51] M. Muniruzzaman,[6] J. Murata,[38,39] S. Nagamiya,[20] J. L. Nagle,[9] T. Nakamura,[14] B. K. Nandi,[6] M. Nara,[48] J. Newby,[46] P. Nilsson,[29] A. S. Nyanin,[23] J. Nystrand,[29] E. O'Brien,[5] C. A. Ogilvie,[16] H. Ohnishi,[5,38] I. D. Ojha,[49,3] K. Okada,[38] M. Ono,[48] V. Onuchin,[15] A. Oskarsson,[29] I. Otterlund,[29] K. Oyama,[8] K. Ozawa,[8] D. Pal,[51] A. P. T. Palounek,[27] V. Pantuev,[44] V. Papavassiliou,[34] J. Park,[42] A. Parmar,[33] S. F. Pate,[34] T. Peitzmann,[30] J.-C. Peng,[27] V. Peresedov,[17] C. Pinkenburg,[5] R. P. Pisani,[5] F. Plasil,[35] M. L. Purschke,[5] A. K. Purwar,[44] J. Rak,[16] I. Ravinovich,[51] K. F. Read,[35,46] M. Reuter,[44] K. Reygers,[30] V. Riabov,[37,40] Y. Riabov,[37] G. Roche,[28] A. Romana,[25] M. Rosati,[16] P. Rosnet,[28] S. S. Ryu,[52] M. E. Sadler,[1] N. Saito,[38,39] T. Sakaguchi,[8,50] M. Sakai,[32] S. Sakai,[48] V. Samsonov,[37] L. Sanfratello,[33] R. Santo,[30] H. D. Sato,[24,38] S. Sato,[5,48] S. Sawada,[20] Y. Schutz,[45] V. Semenov,[15] R. Seto,[6] M. R. Shaw,[1,27] T. K. Shea,[5] T.-A. Shibata,[47,38] K. Shigaki,[14,20] T. Shiina,[27] C. L. Silva,[41] D. Silvermyr,[27,29] K. S. Sim,[22] C. P. Singh,[3] V. Singh,[3] M. Sivertz,[5] A. Soldatov,[15] R. A. Soltz,[26] W. E. Sondheim,[27] S. P. Sorensen,[46] I. V. Sourikova,[5] F. Staley,[10] P. W. Stankus,[35] E. Stenlund,[29] M. Stepanov,[34] A. Ster,[21] S. P. Stoll,[5] T. Sugitate,[14] J. P. Sullivan,[27] E. M. Takagui,[41] A. Taketani,[38,39] M. Tamai,[50] K. H. Tanaka,[20] Y. Tanaka,[32] K. Tanida,[38] M. J. Tannenbaum,[5] P. Tarján,[11] J. D. Tepe,[1,27] T. L. Thomas,[33] J. Tojo,[24,38] H. Torii,[24,38] R. S. Towell,[1] I. Tserruya,[51] H. Tsuruoka,[48] S. K. Tuli,[3] H. Tydesjö,[29] N. Tyurin,[15] H. W. van Hecke,[27] J. Velkovska,[5,44] M. Velkovsky,[44] V. Veszprémi,[11] L. Villatte,[46] A. A. Vinogradov,[23] M. A. Volkov,[23] E. Vznuzdaev,[37] X. R. Wang,[13] Y. Watanabe,[38,39] S. N. White,[5] F. K. Wohn,[16] C. L. Woody,[5] W. Xie,[6] Y. Yang,[7] A. Yanovich,[15] S. Yokkaichi,[38,39] G. R. Young,[35] I. E. Yushmanov,[23] W. A. Zajc,[9,†] C. Zhang,[9] S. Zhou,[7] S. J. Zhou,[51] and L. Zolin[17]

(PHENIX Collaboration)

[1]*Abilene Christian University, Abilene, Texas 79699, USA*
[2]*Institute of Physics, Academia Sinica, Taipei 11529, Taiwan*
[3]*Department of Physics, Banaras Hindu University, Varanasi 221005, India*
[4]*Bhabha Atomic Research Centre, Bombay 400 085, India*

[5]Brookhaven National Laboratory, Upton, New York 11973-5000, USA
[6]University of California–Riverside, Riverside, California 92521, USA
[7]China Institute of Atomic Energy (CIAE), Beijing, People's Republic of China
[8]Center for Nuclear Study, Graduate School of Science, University of Tokyo, 7-3-1 Hongo, Bunkyo, Tokyo 113-0033, Japan
[9]Columbia University, New York, New York 10027, USA and Nevis Laboratories, Irvington, New York 10533, USA
[10]Dapnia, CEA Saclay, F-91191, Gif-sur-Yvette, France
[11]Debrecen University, H-4010 Debrecen, Egyetem tér 1, Hungary
[12]Florida State University, Tallahassee, Florida 32306, USA
[13]Georgia State University, Atlanta, Georgia 30303, USA
[14]Hiroshima University, Kagamiyama, Higashi-Hiroshima 739-8526, Japan
[15]Institute for High Energy Physics (IHEP), Protvino, Russia
[16]Iowa State University, Ames, Iowa 50011, USA
[17]Joint Institute for Nuclear Research, 141980 Dubna, Moscow Region, Russia
[18]KAERI, Cyclotron Application Laboratory, Seoul, South Korea
[19]Kangnung National University, Kangnung 210-702, South Korea
[20]KEK, High Energy Accelerator Research Organization, Tsukuba-shi, Ibaraki-ken 305-0801, Japan
[21]KFKI Research Institute for Particle and Nuclear Physics (RMKI), H-1525 Budapest 114, P.O. Box 49, Hungary
[22]Korea University, Seoul, 136-701, Korea
[23]Russian Research Center "Kurchatov Institute," Moscow, Russia
[24]Kyoto University, Kyoto 606-8502, Japan
[25]Laboratoire Leprince-Ringuet, Ecole Polytechnique, CNRS-IN2P3, Route de Saclay, F-91128, Palaiseau, France
[26]Lawrence Livermore National Laboratory, Livermore, California 94550, USA
[27]Los Alamos National Laboratory, Los Alamos, New Mexico 87545, USA
[28]LPC, Université Blaise Pascal, CNRS-IN2P3, Clermont-Fd, 63177 Aubiere Cedex, France
[29]Department of Physics, Lund University, Box 118, SE-221 00 Lund, Sweden
[30]Institut für Kernphysik, University of Muenster, D-48149 Muenster, Germany
[31]Myongji University, Yongin, Kyonggido 449-728, Korea
[32]Nagasaki Institute of Applied Science, Nagasaki-shi, Nagasaki 851-0193, Japan
[33]University of New Mexico, Albuquerque, New Mexico 87131, USA
[34]New Mexico State University, Las Cruces, New Mexico 88003, USA
[35]Oak Ridge National Laboratory, Oak Ridge, Tennessee 37831, USA
[36]IPN-Orsay, Universite Paris Sud, CNRS-IN2P3, BP1, F-91406, Orsay, France
[37]PNPI, Petersburg Nuclear Physics Institute, Gatchina, Russia
[38]RIKEN (The Institute of Physical and Chemical Research), Wako, Saitama 351-0198, Japan
[39]RIKEN BNL Research Center, Brookhaven National Laboratory, Upton, New York 11973-5000, USA
[40]St. Petersburg State Technical University, St. Petersburg, Russia
[41]Universidade de São Paulo, Instituto de Física, Caixa Postal 66318, São Paulo CEP05315-970, Brazil
[42]System Electronics Laboratory, Seoul National University, Seoul, South Korea
[43]Chemistry Department, Stony Brook University, SUNY, Stony Brook, New York 11794-3400, USA
[44]Department of Physics and Astronomy, Stony Brook University, SUNY, Stony Brook, New York 11794, USA
[45]SUBATECH (Ecole des Mines de Nantes, CNRS-IN2P3, Université de Nantes) BP 20722-44307, Nantes, France
[46]University of Tennessee, Knoxville, Tennessee 37996, USA
[47]Department of Physics, Tokyo Institute of Technology, Tokyo, 152-8551, Japan
[48]Institute of Physics, University of Tsukuba, Tsukuba, Ibaraki 305, Japan
[49]Vanderbilt University, Nashville, Tennessee 37235, USA
[50]Waseda University, Advanced Research Institute for Science and Engineering, 17 Kikui-cho, Shinjuku-ku, Tokyo 162-0044, Japan
[51]Weizmann Institute, Rehovot 76100, Israel
[52]Yonsei University, IPAP, Seoul 120-749, Korea

(Received 7 March 2005; published 16 June 2005)

The first measurement of direct photons in Au + Au collisions at $\sqrt{s_{NN}} = 200$ GeV is presented. The direct photon signal is extracted as a function of the Au + Au collision centrality and compared to next-to-leading order perturbative quantum chromodynamics calculations. The direct photon yield is shown to scale with the number of nucleon-nucleon collisions for all centralities.

DOI: 10.1103/PhysRevLett.94.232301 PACS numbers: 25.75.Dw

One of the most exciting observations from experiments at the Relativistic Heavy Ion Collider (RHIC) is the strong suppression of the yield of hadrons at large transverse momenta ($p_T > 2$ GeV/c) in central Au + Au collisions, as compared to measured yields in $p + p$ collisions scaled by the number of binary nucleon-nucleon collisions [1–4].

Such quenching was predicted to result from the energy loss of hard-scattered partons propagating through the high density matter created in heavy ion collisions [5]. It was later proposed that the observed hadron suppression could be an initial-state effect due to saturation of the initial parton distributions in large nuclei [6]. The high-p_T hadron suppression was not observed in d + Au collisions [7,8]. This indicates that the suppression in Au + Au collisions is due to the extended dense matter in the final state that is absent in d + Au collisions.

Measurement of direct photon production allows more definitive discrimination between initial- and final-state suppression due to the fact that photons, once produced, are essentially unaffected by the surrounding matter. Hence photons produced directly in initial parton scatterings are not quenched unless the initial parton distributions are suppressed in the nucleus. In fact, there may be additional direct photon yield in AA collisions [9] due to various processes such as momentum broadening of the incoming partons, additional fragmentation contributions [10,11], or additional scatterings in the thermalizing dense matter of the final state.

This Letter reports on direct photon production in Au + Au collisions at $\sqrt{s_{NN}} = 200$ GeV with data taken by the PHENIX experiment [12] during the second RHIC run (2001–2002). This analysis used the beam-beam counters (BBC, $3.0 < |\eta| < 3.9$) and the zero degree calorimeter (ZDC) for trigger and event characterization, the electromagnetic calorimeter (EMCal) in the two central arms ($|\eta| \leq 0.35$) to measure the inclusive γ, π^0, and η yields, and the tracking system of the central arms to estimate the charged particle contamination. The EMCal consists of two subsystems: six sectors of lead-scintillator sandwich calorimeter (PbSc) and two sectors of lead-glass Čerenkov calorimeter (PbGl). Located at a radial distance of about 5 m, each sector covers an azimuthal interval of $\Delta\phi \approx 22.5°$. The fine segmentation of the EMCal ($\Delta\phi \times \Delta\eta \sim 0.01 \times 0.01$) ensures that the two photons from a decayed π^0 are well resolved up to transverse momenta of 15–20 GeV/c.

The event centrality was selected by cuts on the correlated distribution of charged particles detected in the BBCs versus energy measured in the ZDC detectors. A Glauber model Monte Carlo combined with a simulation of the BBC and ZDC responses gave an estimate of the associated number of binary collisions ($N_{\rm coll}$) and participating nucleons ($N_{\rm part}$) for each centrality bin (values tabulated in Ref. [3]).

For this analysis a minimum bias trigger sample of 30×10^6 events, also used for the previously published π^0 analysis [3], was combined with a level-2 trigger event sample equivalent to additional 55×10^6 minimum bias events. The level-2 trigger sample was obtained by the use of an EMCal software trigger on highly energetic showers equivalent to the level-1 hardware trigger used in Ref. [13]. The threshold energy of the trigger was set at 3.5 GeV with a resulting trigger efficiency plateau at 100% for single photons above $p_T \approx 5$ GeV/c (6.5 GeV/c) for the PbSc (PbGl). The normalization of the level-2 data sample relative to the minimum bias data sample is accurate to 2%. In the following, the minimum bias result refers to the combined level-2 and minimum bias trigger samples without selection on centrality.

The direct photon yield is extracted on a statistical basis, without isolation cuts, by a comparison of the inclusive photon spectra to the expected background from hadronic decays [14,15] (mainly $\pi^0 \rightarrow 2\gamma$). Photonlike clusters are identified in the EMCal by applying appropriate particle identification (PID) cuts based on time of flight and the shower profile. The consistency of the final results obtained independently with the PbSc and PbGl, and with different PID cuts, including no PID cut, is used to check the systematic error estimates. The π^0 and η yields are determined as described in [3,16] by an invariant mass analysis of photon pairs, with the combinatorial background established by combining uncorrelated photon pairs from different events.

The raw inclusive photon-candidate spectra must be corrected for charged and neutral hadron contaminations not removed by the PID cuts, as well as for photon conversions. Charged contaminants are identified by associating photon candidates in the EMCal with charged hits in the pad chamber (PC3) positioned directly in front of the EMCal. The charged contaminant spectra are subtracted from the photon-candidate spectra. The charged hadron contamination depends strongly on the PID cut and increases significantly for $p_T < 3$ GeV/c with a contribution of 4% above 3 GeV/c for the tightest PID cut. The contamination of neutral hadrons (mainly antineutrons) is determined with a full GEANT simulation of the detector response to neutrons and antineutrons with input spectra based on the proton and antiproton yields measured by PHENIX [4]. The neutral hadron contamination is found to be negligible above $p_T = 5$ GeV/c ($< 1\%$). The neutral photon-candidate spectra are corrected for conversions removed by the charged contaminant subtraction with a p_T-independent factor (5.9%–7.3% for different sectors based on simulation).

The raw spectra are normalized to one unit of rapidity and full azimuth (the purely geometrical acceptance correction is $\sim 1/0.35$). The spectra are further corrected for (i) the detector response (energy resolution, dead areas), (ii) the reconstruction efficiency (PID cuts), and (iii) occupancy effects (cluster overlaps). These corrections are quantified by embedding simulated single γ's, π^0's, or η's from a full PHENIX GEANT simulation into real events and by analyzing the merged events with the same analysis cuts used to obtain the real yields. The overall π^0 yield correction was ~ 2.5 with a centrality dependence of $\lesssim 25\%$. The losses were dominated by fiducial and asym-

metry cuts. The nominal energy resolution was adjusted in the simulation by smearing the energies with a constant term of ~5% for PbSc and ~7% for PbGl to reproduce the measured width of the π^0 peak observed at each p_T. The shape, position, and width of the π^0 peak measured for all centralities were confirmed to be well reproduced by the embedded data.

The energy calibration of the EMCal was corroborated by the position of the π^0 invariant mass peak, by the energy deposit from minimum ionizing charged particles traversing the EMCal (PbSc), and by the correlation between the measured momentum of electron and positron tracks identified by the ring-imaging Čerenkov detector and the associated energy deposit in the EMCal. From these studies it is determined that the accuracy of the energy measurement was better than 1.5%.

The main sources of systematic errors in the PbSc and PbGl measurements are the uncertainties in (i) the yield extraction, (ii) the yield correction, and (iii) the energy scale. The relative contributions of these effects to the total error differ for the PbSc and PbGl (Table I). The weighted average of the two independent measurements reduces the total error. The final systematic errors on the spectra are at the level of ~15%–20% (Table I). A correction for the true mean value of the p_T bin is applied to the steeply falling spectra.

TABLE I. Summary of the dominant sources of systematic errors on the π^0 and inclusive γ yields extracted independently with the PbGl and PbSc electromagnetic calorimeters. The error estimates are quoted at two p_T values in central events for the PbGl and PbSc. For the combined π^0 and inclusive γ spectra and γ/π^0 ratios, the approximate statistical and systematical errors are quoted for the most peripheral and most central reactions.

	PbGl (Central)		PbSc (Central)	
π^0 error source	3 GeV/c	8.5 GeV/c	3 GeV/c	8.5 GeV/c
Yield extraction	8.7%	7.0%	9.8%	7.2%
Yield correction	12.1%	12.0%	10.3%	12.5%
Energy scale	13.8%	14.1%	10.5%	11.4%
Total systematic	20.3%	19.8%	17.7%	18.4%
Statistical	10.6%	32.5%	2.1%	10.5%
Inclusive γ error				
Non-γ correction	2.4%	2.4%	3.2%	3.2%
Yield correction	10.2%	12.0%	9.1%	12.5%
Energy scale	15.7%	13.7%	12.4%	10.8%
Total systematic	18.9%	18.4%	15.7%	16.8%
Statistical	1.2%	14.1%	0.6%	4.1%
γ/π^0 syst.	13.6%	12.6%	14.0%	13.4%
γ/π^0 stat.	10.7%	35.4%	2.2%	11.3%
Total errors PbGl and PbSc combined				
	Peripheral		Central	
Error	3 GeV/c	8.5 GeV/c	3 GeV/c	8.5 GeV/c
π^0 syst.	13.2%	17.0%	13.9%	16.1%
π^0 stat.	3.0%	35.3%	1.8%	9.6%
γ syst.	11.4%	15.6%	11.5%	15.9%
γ stat.	3.0%	28.8%	0.6%	3.8%
γ/π^0 syst.	9.9%	13.1%	9.7%	11.2%
γ/π^0 stat.	4.2%	45.6%	1.9%	10.3%
γ/π^0 bkg calc.	4%		4%	

The completely corrected and combined PbSc and PbGl inclusive photon yields are compared to the expected yields of background photons from hadronic decays in Fig. 1 for minimum bias Au + Au collisions (0%–92% of the geometric cross section) and for five centrality bins. The decay photon calculations are based on the measured π^0 and η spectra [16] assuming m_T scaling for all other radiative decays (η', K^0_s, ω). The comparison is made as the ratio of measured (inclusive) γ/π^0 and calculated background γ/π^0 since this has the advantage that many uncertainties, such as the energy scale, cancel to a varying extent in the ratio. Since the π^0 spectra of the background calculations are taken to be the same as the measured spectra, we have

$$R_\gamma = \frac{(\gamma/\pi^0)_{\text{Measured}}}{(\gamma/\pi^0)_{\text{Background}}} \approx \frac{\gamma_{\text{Measured}}}{\gamma_{\text{Background}}}, \qquad (1)$$

and any significant deviation of the double ratio above unity indicates a direct photon excess. In Fig. 1 an excess

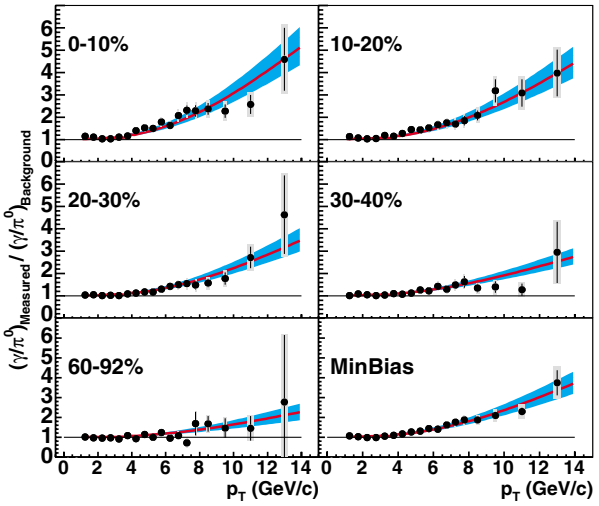

FIG. 1 (color online). Double ratio of measured $(\gamma/\pi^0)_{\text{Measured}}$ invariant yield ratio to the background decay $(\gamma/\pi^0)_{\text{Background}}$ ratio as a function of p_T for minimum bias and for five centralities of Au + Au collisions at $\sqrt{s_{NN}} = 200$ GeV (0%–10% is the most central). Statistical and total errors are indicated separately on each data point by the vertical bar and shaded region, respectively. The solid curves are the ratio of pQCD predictions described in the text to the background photon invariant yield based on the measured π^0 yield for each centrality class. The shaded regions around the curves indicate the variation of the pQCD calculation for scale changes from $p_T/2$ to $2p_T$, plus the $\langle N_{\text{coll}} \rangle$ uncertainty.

is observed at high p_T with a magnitude that increases with increasing centrality of the collision.

The measured results are compared to NLO perturbative QCD (pQCD) predictions [17], scaled by the number of binary nucleon collisions for each centrality selection. The same calculations are in agreement with the PHENIX direct photon measurement [15] for $p + p$ collisions at the same $\sqrt{s}$, and similar NLO pQCD calculations provide a good description of the measured π^0 production in $p + p$ collisions [13]. The calculations were performed [15,17] with normalization and factorization scales set equal to p_T, and using the CTEQ6 [18] set of parton distribution functions and the GRV set of fragmentation functions [19]. The direct photon spectra extracted as $\gamma_{\text{Direct}} = (1 - R_\gamma^{-1}) \cdot \gamma_{\text{Measured}}$ are shown in Fig. 2 for all nine centrality selections as well as minimum bias, and compared to the same NLO calculations. The binary collision scaled predictions are seen to provide a good description of the measured direct photon spectra (Fig. 2). The increasing ratio with centrality seen in Fig. 1 is therefore attributed to the decreasing decay background due to π^0 suppression [3].

Medium effects in AA collisions are often presented using the *nuclear modification factor* given as the ratio of the measured AA invariant yields to the NN-collision-scaled $p + p$ invariant yields:

$$R_{AA}(p_T) = \frac{(1/N_{AA}^{\text{evt}}) d^2N_{AA}/dp_T dy}{\langle N_{\text{coll}}\rangle/\sigma_{pp}^{\text{inel}} \times d^2\sigma_{pp}/dp_T dy}, \qquad (2)$$

where the $\langle N_{\text{coll}}\rangle/\sigma_{pp}^{\text{inel}}$ is the average nuclear thickness function, $\langle T_{AA}\rangle$, in the centrality bin under consideration (Ref. [3]). $R_{AA}(p_T)$ measures the deviation of AA data from an incoherent superposition of NN collisions.

The centrality dependence of the high p_T γ production represented as a function of the number of participating nucleons, N_{part}, is shown by the closed circles in Fig. 3. The production in Au + Au collisions relative to $p + p$ is characterized by the $R_{AA}(p_T > 6\ \text{GeV}/c)$ ratio of Eq. (2) as the ratio of Au + Au over the $\langle N_{\text{coll}}\rangle$ scaled $p + p$ yields each integrated above 6 GeV/c. The direct photon $p + p$ yields are taken as the NLO pQCD predictions described above. As noted above, the high p_T direct γ production is well described by the $p + p$ direct γ yield prediction scaled by $\langle N_{\text{coll}}\rangle$ for all centralities. This is in sharp contrast [3] to the centrality dependence of the π^0 $R_{AA}(p_T > 6\ \text{GeV}/c)$ shown by open circles in Fig. 3 where the measured π^0 yield [13] is used as the $p + p$ reference in Eq. (2).

The observed close agreement between the measured yields and NLO calculations is in contrast to observations for central Pb + Pb collisions at $\sqrt{s_{NN}} = 17.3$ GeV [14] where the measured photon yield exceeds the scaled NN photon yield by about a factor of 2. The present result constrains modifications of the initial parton distributions, or of the fragmentation contributions [10,11] (in these

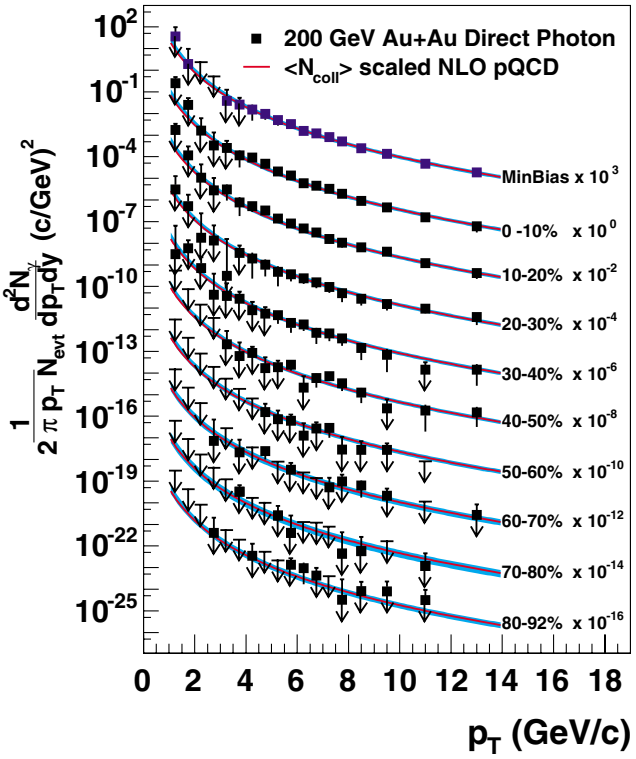

FIG. 2 (color online). Direct γ invariant yields as a function of transverse momentum for 9 centrality selections and minimum bias Au + Au collisions at $\sqrt{s_{NN}} = 200$ GeV. The vertical error bar on each point indicates the total error. Arrows indicate measurements consistent with zero yield with the tail of the arrow indicating the 90% confidence level upper limit. The solid curves are pQCD predictions described in the text.

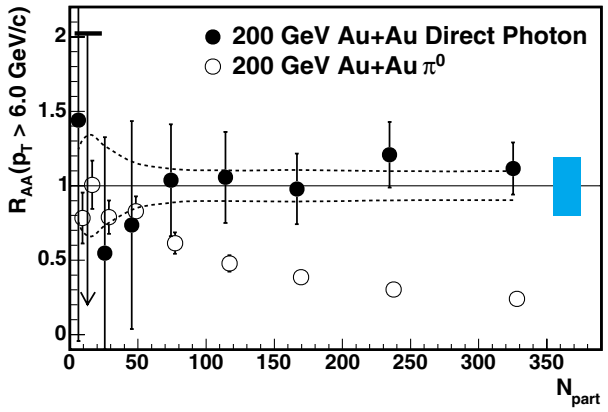

FIG. 3 (color online). Ratio of Au + Au yield to $p + p$ yield normalized by the number of binary nucleon collisions as a function of centrality given by N_{part} for direct γ (closed circles) and π^0 (open circles) yields integrated above 6 GeV/c. The $p + p$ direct photon yield is taken as the NLO pQCD prediction described in the text. The error bars indicate the total error excluding the error on $\langle N_{\text{coll}}\rangle$ shown by the dashed lines and the scale uncertainty of the NLO calculation shown by the shaded region at the right.

NLO calculations the contribution is significant: ~50% at 3.5 GeV/c and ~35% at 10 GeV/c), or additional photon yield from thermal radiation to levels comparable to the present measurement uncertainty.

In summary, the transverse momentum spectra of direct photons have been measured at midrapidity up to $p_T \approx 13$ GeV/c for nine centrality bins of Au + Au collisions at $\sqrt{s_{NN}} = 200$ GeV. The significance of the direct photon signal increases with collision centrality due to the increasingly suppressed π^0 production and associated decrease in the photon background from hadron decays. The direct photon spectral shapes and invariant yields are consistent with NLO pQCD predictions for $p + p$ reactions scaled by the average number of inelastic NN collisions for each centrality class. The close agreement between measurement and the binary scaled pQCD predictions of the direct photon yield suggests that nuclear modifications of the quark and gluon distribution functions in the relevant region of momentum fraction x are minor. The result provides strong confirmation that the observed large suppression of high p_T hadron production in central Au + Au collisions is dominantly a final-state effect due to parton energy loss in the dense produced medium, rather than an initial-state effect.

We thank the staff of the Collider-Accelerator and Physics Departments at BNL for their vital contributions. We acknowledge support from the Department of Energy and NSF (U.S.A.), MEXT and JSPS (Japan), CNPq and FAPESP (Brazil), NSFC (China), CNRS-IN2P3 and CEA (France), BMBF, DAAD, and AvH (Germany), OTKA (Hungary), DAE and DST (India), ISF (Israel), KRF and CHEP (Korea), RMIST, RAS, and RMAE (Russia), VR and KAW (Sweden), U.S. CRDF for the FSU, U.S.-Hungarian NSF-OTKA-MTA, and U.S.-Israel BSF.

*Deceased.
†PHENIX Spokesperson.
Electronic address: zajc@nevis.columbia.edu

[1] K. Adcox *et al.*, Phys. Rev. Lett. **88**, 022301 (2002).
[2] C. Adler *et al.*, Phys. Rev. Lett. **89**, 202301 (2002).
[3] S. S. Adler *et al.*, Phys. Rev. Lett. **91**, 072301 (2003).
[4] S. S. Adler *et al.*, Phys. Rev. C **69**, 034909 (2004).
[5] M. Gyulassy and M. Plumer, Phys. Lett. B **243**, 432 (1990).
[6] D. Kharzeev, E. Levin, and L. McLerran, Phys. Lett. B **561**, 93 (2003).
[7] S. S. Adler *et al.*, Phys. Rev. Lett. **91**, 072303 (2003).
[8] J. Adams *et al.*, Phys. Rev. Lett. **91**, 072304 (2003).
[9] T. Peitzmann and M. H. Thoma, Phys. Rep. **364**, 175 (2002).
[10] R. J. Fries, B. Muller, and D. K. Srivastava, Phys. Rev. Lett. **90**, 132301 (2003).
[11] B. G. Zakharov, JETP Lett. **80**, 1 (2004).
[12] K. Adcox *et al.*, Nucl. Instrum. Methods Phys. Res., Sect. A **499**, 469 (2003).
[13] S. S. Adler *et al.*, Phys. Rev. Lett. **91**, 241803 (2003).
[14] M. M. Aggarwal *et al.*, Phys. Rev. Lett. **85**, 3595 (2000).
[15] S. S. Adler *et al.*, Phys. Rev. D **71**, 071102 (2005).
[16] S. S. Adler *et al.* (to be published). An η/π^0 ratio of $R_{\eta/\pi^0}(p_T \to \infty) = 0.45 \pm 0.05$ has been used.
[17] L. E. Gordon and W. Vogelsang, Phys. Rev. D **48**, 3136 (1993).
[18] J. Pumplin *et al.*, J. High Energy Phys. 07 (2002) 012.
[19] M. Gluck, E. Reya, and A. Vogt, Phys. Rev. D **48**, 116 (1993).